

Hats off to Exoplanet HAT-P-6b's imperceptible Transit

114995854 AND 114380964, 115282553¹

¹*Department of Physics and Astronomy, Stony Brook University*

(Dated: 4th of November, 2024)

ABSTRACT

This report details a photometric observation of the exoplanet HAT-P-6b transiting its host star HAT-P-6, using the 14-inch telescope at Mt.Stony Brook Observatory on October 5th, 2024, with a blue filter which best suited HAT-P-6. The experiment aimed to confirm the existence of the exoplanet HAT-P-6b by measuring the host star's change in relative flux during an expected period when the exoplanet's transit crosses our Telescope's line of sight. Through data analysis, which included CCD imaging, flat-field, bias, and dark calibration, and aperture photometry, we resulted in a measured transit depth of approximately 10.06 ± 13.91 ppt, with a 1% change in measured relative flux. Although these values are relatively reasonable, and close to the literature, as we will discuss later on, we are unable to conclude the detection of an exoplanet, measure proper depth of transit and a radius value for HAT-P-6b, due to potentially fundamental issues with our measured photometric data.

1. INTRODUCTION

1.1. *scientific motivation*

exoplanets are planets that orbit stars outside of our Solar System. They provide valuable insight into planetary information such as formation, composition, and comparison to our beloved blue rock. Detection of these exoplanets, given their size, composition, and distance, is extremely difficult and improbable. However, there have been established telescopic methods to still detect these covert objects given these constraints.

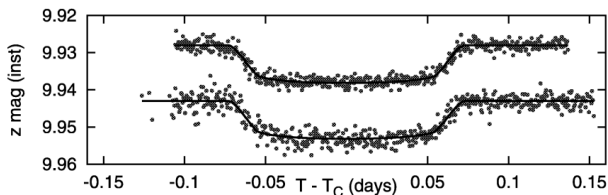
Photometric imaging of stars that we expect to host orbiting exoplanets can potentially allow us to detect them. By predicting a potential time frame that the transiting planet crosses the star along our line of sight, we can take a series of photometric images in filters specific to the star's spectral type, in order to measure potential changes in the star's relative flux. Changes in flux or brightness at a predicted time frame can result in implications of a orbiting exoplanet, and even allow us to calculate important information such as planetary composition, radius, and more.

One may question the probability of finding a host star, with a potential exoplanet, matching up its transit to our line of sight as it crosses across the Star's surface. However, the sheer population of stars in our Galaxy alone terminates the low probability [Birrner \(n.d.\)](#). Our target star (and planet), HAT-P-6 and Hat-P-6b are a dynamic duo located in the Andromeda galaxy [Noyes et al. \(2008\)](#). HAT-P-6b, is in a class of exoplanet known as "hot Jupiters", which are a classification of exoplanets that are comparable in composition and size to Jupiter, but orbit extremely close to their host stars, leading to extremely high temperatures, larger radii, and compositional differences [Charbonneau et al. \(2000\)](#). HAT-P-6's relatively similar density and mass to Jupiters (*1.6 Jupiter masses*), but puffed up radius (*1.33 Jupiter Radii*), makes it an interesting case study as we can study the effects of extreme stellar radiation on its "puffy" atmosphere. [Noyes et al. \(2008\)](#) Although that is much beyond the scope of this experiment :).

1.2. *Experimental goals*

In this lab we aim to confirm the existence of HAT-P-6b, thereafter calculating its radius and transit depth, through the 'photometric transit method'. This method entails taking a larger series of photometric images of a host star, aiming to capture the passing transit of a orbiting exoplanet relative to our line of sight, which allows us to measure the relative flux of the star by constructing a time dependent light curve. And identify dips or diminishes in the flux, implying that a exoplanet

Figure 1. Example light curve (R. W. Noyes)



exists based on expected percent change of 1% in the flux count. Since our exoplanet is confirmed to exist, we can calculate and predict viewing its transit across the host star along our line of sight. This photometry detection method allows us to bypass the struggles of detecting exoplanets that are comparatively tiny to their host stars and hold vast differences in brightness.

We chose HAT-P-6b in leu of variables such as time constraints (within the first week of October where the peak transit was at a reasonable time in the night), favorable weather conditions, and an apparent magnitude of 10.54.

the next section, Observations and Data, will entail the experimental design, data acquisition, unique complications/issues, and data descriptions. We will then detail our data reduction, analysis, and troubleshooting in section three, and will complete the papers with our results and their implications and discussions in section 4.

2. OBSERVATIONS AND DATA

2.1. *Experimental setup*

The experimental setup entails primarily finding our exoplanet in an [exoplanet catalog](#) linked here, which identifies transiting planets at certain dates, times, and more info. But the transit depth, transit midpoints, and duration have to be calculated. Our group researched online and discovered a different website/catalog called [astro.swarthmore](#) which provides all the needed info like RA/DEC magnitude, period, and other relevant info such as transit duration, midpoints, and depth. Through this we chose three primary stars, however due to weather conditions and scheduling constraints, we conducted our experiment on the 5th of October for HAT-P-6, which was our backup star. We also created Finder charts (slightly larger than the Telescope's F.O.V of 23.69') and Star Alt Plots to help properly locate the target in the telescope during calibration. we took our calibration files: darks, bias, and flats, at the end after we took our science images of the transit, in order to use the same exposures for calibration and imaging data, which was decided after testing different exposures in real time

Our duration at the Mt. Stony Brook observatory lasted from 7pm to 2 am. The first two hours consisted of setting up the telescope, which included hooking up our CCD camera - we used a SBIG STL-1001E - to our telescope, a 14-inch Meade LX200-ACF telescope which rests on a Mesu-200 German Equatorial Mount [Birrer](#) (????). We operated the CCD Camera and Telescope from a windows machine that has CCD Soft, Cartes De Ciel, and other relevant applications. Once our setup

was connected and ready to go, we begun by locating the star. We experienced a large delay in tracking

Figure 2. Overall Finder Chart For HAT-P-6

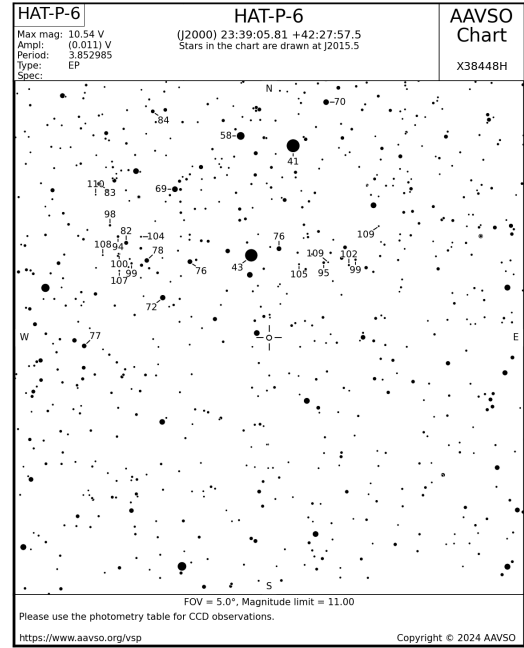
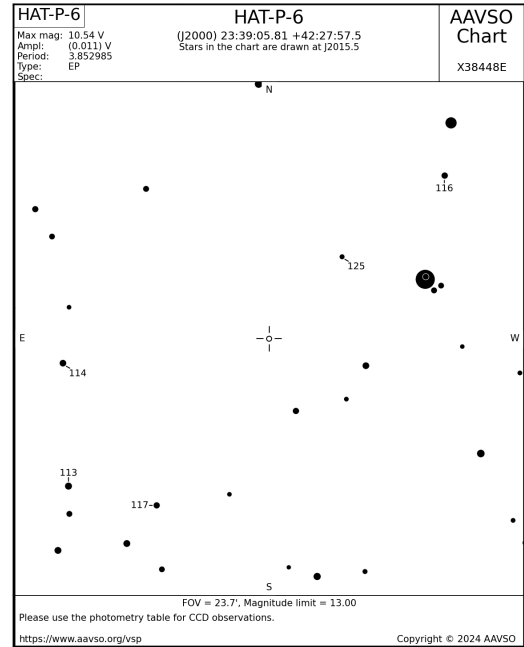


Figure 3. Finder Chart for Finder scope of telescope




the star, the telescope was not left properly calibrated so as a result it was consistently looking in the wrong region despite our commands to align to a certain star or

galaxy. We also had misplaced plugging in the laptop to WiFi (Ethernet cable), so Cartes De Ciel was not working properly as it could not identify the current real time which meant the telescope was not positioned where the program said it was. After manually aligning using reference stars whose coordinates we were certain of, and plugging in the laptop to the Ethernet, we were able to correctly align ourselves with HAT-P-6 using our finder charts.

2.2. Experimental design and Data-taking

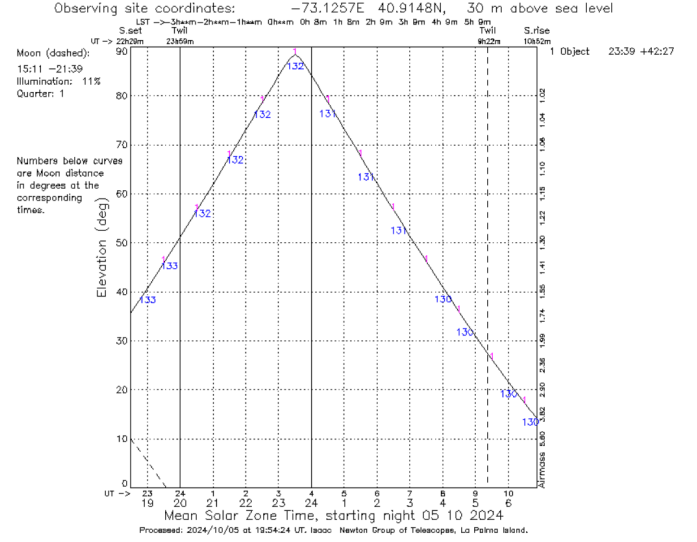
We will detail the experimental plan and process for the data taking in this section. Our program involves taking a long series of photometric images before, during, and after the transit in order to process the baseline flux as well as the variable flux during the predicted transit times. We decided to take our calibration images after taking our transit data. We will be working in the blue filter, HAT-P-6's spectral type is F, but after testing both red and blue filters, we found that blue aligns better for higher resolved images. Another note, by maintaining HAT-P-6 in the center, we can obtain several stars that will be used for flux calibrations, and help to correct for atmospheric changes as well as variability of stellar brightness (More on this in the data analysis). The specifics of the HAT-P-6b transit were as follows in the star alt and transit finder images provided below in Figure 4.

Figure 4. Transit information

Search: <input type="text"/>		Show if visible transit % + baseline % > 0 <input checked="" type="checkbox"/> <input type="checkbox"/> <input type="checkbox"/> <input type="checkbox"/> <input type="checkbox"/> <input type="checkbox"/> <input type="checkbox"/> <input type="checkbox"/> <input type="checkbox"/> <input type="checkbox"/> <input type="checkbox"/>										Other Site	
Local evening date	Name	V or Gaia mag	Start—Mid—End	Duration	BJD _{TDB} start—mid—end	Elev. at start, mid, end ±1 hrs	% of transit (baseline) observable, Suggested obs. start, end	Az. at start, mid, end ±1 hrs	HA at start, mid, end ±1 hrs	RA & Dec (J2000)	Period (days)	Depth (ppt)	Comments
Sat. 2024-10-05: Nautical twilight 2024-10-05 19:26 — 2024-10-06 05:55 local time / 2024-10-05 23:26 — 2024-10-06 09:55 UTC													
Sat. 2024-10-05 Nautical twilight 19:26 – 05:55 (EST/EDT)	<input type="checkbox"/> HAT-P-6 b Finding charts: Annotated , Aladin , SkyMap , Airmass plot , ACP plan Info: Exoplanet Archive , Simbad , Gaia , TIC	10.5 Moon 10% @133°	20:13 21:13—22:54 —00:35 01:36 ±0:01	3:22	10589.5562 10589.6262 10589.6962	53° 64°, 83°, 78° 67°	 100% (100%) 20:13—01:36	70° 75°, 73°, 283° 285°	-3.3 -2.3, -0.6, +1.1 +2.1	23:39:05.78 +42:27:57.55	3.85	9.1	

the catalog (Figure 4) is above from the astro.swarthmore website conducting a catalog search of exoplanets, above is the information for our exoplanet. Our duration lasted a total of 3 hours and 22 minutes starting at 9:13 pm and ending at 12:35 am, with our transient midpoint at 10:54 pm. The moon was quite low and very little illumination was present indicated by both the star alt plot (Figure 5) as well as the transit finder catalog. As for weather conditions, we experienced essentially 0 cloud coverage visible to the naked

Figure 5. Transit information



eye. Forecasts also predicted 0 cloud coverage during our hours of recording. Due to the complications with the telescope, by the time our star was located, it was around 10:50 pm, and our first "calibrated" science image was not until 10:59 pm. By "calibrated", we mean testing different filters and concluding on the blue, and taking different level exposures in order to stay well below saturation levels while still maintaining high Signal-To-Noise Ratio. Our final selected exposure time was 18 seconds for around 300 science images. Below in Table 1 is a summary of our data run.

Table 1. Summary of Observation Frames

Frames	# of Exposures	Exposure time (s)	Filter	AutoDark
Science Images	300	18 s	Blue	Off
Dark Frames	10	.5 s	N/A	Off
Flat Frames	10	.5 s	Blue	On

Our recorded calibration files were flat fields (in the blue filter) and dark frames, both post transit imaging. These encompass our needed files to correct any read out noise, pixel sensitivity, vignetting, and of course dust/dirt on the telescope. The dark frames already incorporate the bias frames into them as they are just a measure of electric noise which is a part of the read out noise.

Our data required a few adjustments in that we encountered the need to carry out a meridian flip during imaging of the transit because of the angle at which HAT-P-6 was high in the sky. So between 11:30-11:45 we flipped the telescope and relocated HAT-P-6. This led to a loss of about 40 data frames from our original 300. We also had to move the dome for this process, which was done prior at 11:08 pm, losing only one frame in the 20s range. We also experienced a small shifting of every image that was taken as the night progressed, slowly but surely shifting our selected star and references out of frame. So this called for us to monitor and move the star and its generally visible references if they moved to far off towards the edge. This move happened for around 5 frames during 12:14 - 12:17 which is slightly before the end of the transit. The telescope experienced a second similar move, losing only one frame, at 12:33. This will be discussed further during data analysis and results as it has potentially larger implications on the nature of our overall light curve and data itself.

3. DATA ANALYSIS

In This section we detail our overall Data Analysis of the obtained, including reduction, image solving and extracting sources, light curve creation, and final reductions for our target light curve, as well as radius and transit depth calculations

3.1. data reduction

We begin our data analysis by primarily correcting the images from intrinsic factors that all telescope users have to deal with. Factors like readout and electrical noise, vignetting, dust/dirt, and pixel sensitivity are just a few variables that our images pick up, but can be corrected by calibration-al images. Dark frames, images taken at certain exposures with a closed shutter, allow us to measure overall readout noise: statistical electric noise (also known as bias frames - 0 exposure images) and noise due to thermal fluctuations. Flat fields are images taken at even illumination sources, maintaining same exposures as our science images, in order to capture the effects of vignetting, pixel variability, and dust/dirt on the telescope and camera.

We took 10 dark frames, and 10 flat field frames for the purpose of calibration. They were both at .5 second

exposures, it is important for the dark frames and flat fields to be uniform in exposures in order to make sure that we don't over or under correct the pixel variations of the flat fields. We started off by taking the median combine of our dark frames by stacking our 10 images in a 3D array, and finding the median pixel value at each position. [Median combines preserve skew quality much better than averages, as they are not subject to variability from large outliers] We then take the same median combine for our 10 flat field images, and then we normalize our flat fields. Normalization makes them universally applicable, independent of exposure times or brightness levels. We accomplish this by dividing out the median value of the difference of the master flats and darks, from their difference.

$$Flat_{Master_{norm}} = \frac{Flat_{Master} - Dark_{Master}}{Median[Flat_{Master} - Dark_{Master}]} \quad (1)$$

we then finally calibrated our science images using the master dark frames and normalized flat fields. This is done by taking the difference of each image with the master dark frame, and dividing out the normalized flat field, giving us our calibrated science images, correcting intrinsic noise, dust, vignetting, and other variations.

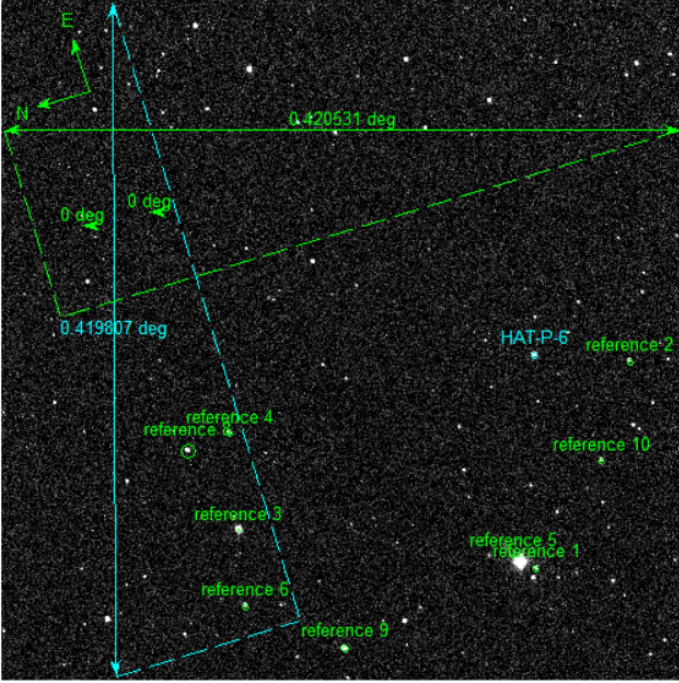
$$Science_{calibrated} = \frac{Science - Dark_{Master}}{Flat_{Master_{norm}}} \quad (2)$$

3.2. Astrometry-Image alignment

Once we obtained our Calibrated photometric images, we then shifted focus to our stars, first we had to locate them in all 300 images. [Astrometry](#) provides a website where this can be done, writing a WCS to the file header. A WCS, or World Coordinate System, is used often in astronomy to correlate pixel coordinates to celestial coordinate such as Right Ascension and Declination. [Greisen & Calabretta \(2002\)](#). This allows us to locate images and find not only our target star, but referential ones for flux calibration as well, given that our star. However, running ~ 300 images individually in the web version would be painstakingly slow. So instead we used the solve-field, a command line tool available from the Astrometry.net package that is installable from Linux/Unix machines. We ran ours on a WSL (windows subsystem for Linux), *does not run on python* with some bash-scripting provided by the AST443/PHY517 Wiki Page [Birrer \(???\)](#). Solve-Field requires a general RA and DEC information, as well index files, which are made available for download on [their website](#). The specific index files needed can be verified by running the website version which tells the specific index file was used. Index files are essentially star catalogs and what astrometry used to pattern match uploaded fits files by

celestial coordinates. Below is a image containing all our chosen reference stars by RA and DEC including HAT-P-6, and the file's WCS header:

Figure 6. Transit information



Now onto Source Extractor (commonly known as SExtractor). This is another program that can be used in order build catalogs containing information for each image; importantly for us, celestial coordinates, flux, and times. In order to identify the fluxes of our references stars, we have to specify certain sized circular apertures for each star to help reduce background noise and illumination from other stars and objects. This helps maintain a constant flux count across that specific star pixels. Our lab manual suggests creating these aperture radii by hand in ds9, so we picked out 10 reference stars that were similar in brightness. we ran our packaged code two different times: once with a 6 pixel aperture radius, and a second time with a 11 pixel aperture radius. This was because the 6 pixel radius assumes a very tight fit, and to give leeway for atmospheric conditions and variable seeing, Telescope drifting, and improved Signal-To-Noise Ratio as our stars were all relatively dim, around the scope of our 10.5 Magnitude target star. (More on why later in section 4)

our resulting .csv files created by SExtractor were formatted quite odd, where all the column and row titles come out as a list together, and then the data as a 2nd following list. So we defined a function in order to reformat each data frame by defining the column titles and manually placing the data from already given "list-like" formatting. Here is the outputted proper example data frame above:

Figure 7. Transit information

```

SIMPLE      =          T / conforms to FITS standard
BITPIX      =         -64 / array data type
NAXIS       =          2 / number of array dimensions
NAXIS1      =         1024
NAXIS2      =         1024
EXTEND      =          T
COMMENT     Original key: "END"
COMMENT
COMMENT     --Start of Astrometry.net WCS solution--
COMMENT     --Put in by the new-wcs program--
COMMENT
WCSAXES     =          2 / no comment
CTYPE1      = 'RA---TAN-SIP' / TAN (gnomic) projection + SIP distortions
CTYPE2      = 'DEC--TAN-SIP' / TAN (gnomic) projection + SIP distortions
EQUINOX     =        2000.0 / Equatorial coordinates definition (yr)
LONPOLE     =         180.0 / no comment
LATPOLE     =          0.0 / no comment
CRVAL1      =        354.79067635 / RA of reference point
CRVAL2      =        42.5588902474 / DEC of reference point
CRPIX1      =        574.945556641 / X reference pixel
CRPIX2      =        454.612136841 / Y reference pixel
CUNIT1      = 'deg' / X pixel scale units
CUNIT2      = 'deg' / Y pixel scale units
CD1_1       =       -0.000119897073224 / Transformation matrix
CD1_2       =        0.000397619357086 / no comment
CD2_1       =       -0.000397641765898 / no comment
CD2_2       =       -0.000119965590371 / no comment
IMAGEW      =        1024 / Image width, in pixels.
IMAGEH      =        1024 / Image height, in pixels.
A_ORDER     =          2 / Polynomial order, axis 1
A_0_0       =          0 / no comment
A_0_1       =          0 / no comment
A_0_2       =       -2.79234488563E-07 / no comment
A_1_0       =          0 / no comment
A_1_1       =       -5.19446341019E-07 / no comment
A_2_0       =       -3.00548014607E-07 / no comment
B_ORDER     =          2 / Polynomial order, axis 2
B_0_0       =          0 / no comment
B_0_1       =          0 / no comment
B_0_2       =        4.26373449899E-07 / no comment

```

3.3. Source Extractor - Aperture photometry

Now onto Source Extractor (commonly known as SExtractor). This is another program that can be used in order build catalogs containing information for each image; importantly for us, celestial coordinates, flux, and times. In order to identify the fluxes of our references stars, we have to specify certain sized circular apertures for each star to help reduce background noise and illumination from other stars and objects. This helps maintain a constant flux count across that specific star pixels. Our lab manual suggests creating these aperture radii by hand in ds9, so we picked out 10 reference stars that were similar in brightness.

we ran our packaged code two different times: once with a 6 pixel aperture radius, and a second time with a 11 pixel aperture radius. This was because the 6 pixel radius assumes a very tight fit, and to give leeway for atmospheric conditions and variable seeing, Telescope drifting, and improved Signal-To-Noise Ratio as our stars were all relatively dim, around the scope of

our 10.5 Magnitude target star. (More on why later in section 4)

our resulting .csv files created by SExtractor were formatted quite odd, where all the column and row titles come out as a list together, and then the data as a 2nd following list. So we defined a function in order to reformat each data frame by defining the column titles and manually placing the data from already given "list-like" formatting. Here is the outputted proper example data frame below:

Figure 8. sextractor, formatted .csv data frame

	object_index	x	y	barycenter_ra	barycenter_dec	\
0	1	172.7031	18.8505	354.604129	42.766910	
1	2	336.6120	6.5920	354.570925	42.703148	
2	3	422.4013	1.2324	354.554146	42.669646	
3	4	272.9149	1008.1302	355.122703	42.607976	
4	5	785.7020	1004.1550	355.036160	42.404770	
..	
185	186	563.8896	29.2798	354.546458	42.610002	
186	187	55.4124	20.7747	354.624216	42.813348	
187	188	765.9554	1017.3782	355.046515	42.411012	
188	189	482.2494	14.9886	354.551916	42.644192	
189	190	839.6770	1009.4879	355.030176	42.382680	

	aperture_flux	aperture_flux_error	time	flux_radius	gaussian_fwhm	\
0	5863.5820	104.59510	0.057	1.395	2.62	
1	1506.0660	104.28110	0.057	1.388	2.65	
2	1353.6380	79.32045	0.057	0.967	2.24	
3	35907.1200	104.53970	0.057	1.365	2.66	
4	965.4219	104.55820	0.057	0.610	0.72	
..	
185	275.7545	104.55820	0.057	1.288	3.66	
186	468.6716	104.44750	0.057	1.339	4.64	
187	1379.5200	104.44750	0.057	1.439	3.35	
188	601.6802	104.42900	0.057	1.285	3.40	
189	960.1848	104.57660	0.057	1.490	3.35	

	background	threshold	flux_max	isoarea_image	prof_rms_major_axis	\
0	61.26605	24.55094	737.50240	32.0	1.186	
1	60.47659	24.55094	181.65110	17.0	1.056	
2	60.47929	24.55094	286.29030	9.0	1.066	
3	61.22442	24.55094	4695.07600	58.0	1.313	
4	61.17706	24.55094	556.90520	5.0	0.515	
..	
185	60.26543	24.55094	44.88363	5.0	0.828	
186	60.91049	24.55094	58.96896	10.0	1.217	
187	61.21399	24.55094	149.40260	17.0	1.214	
188	60.47740	24.55094	67.82427	11.0	1.075	
189	61.24632	24.55094	132.51650	16.0	1.131	

	prof_rms_minor_axis	pos_angle	flags
0	1.038	-62.05	0
1	0.896	-41.39	16
2	0.418	-3.44	24
3	1.047	-51.37	0
4	0.362	-1.36	0
..
185	0.466	-52.34	0
186	0.698	-62.22	0
187	0.835	-70.78	16
188	0.677	-19.02	0
189	0.990	-85.92	0

Once our data frames were made, we could configure out data frames to create light curve based data frames for our reference stars. however in order to automate the process, we decided to provide the RA and DEC, and identify if a star is found within a very small specified radius or aperture field, this prevents partial findings from being identified as stars, and also uses known co-ordinates for the stars to guarantee our star is being used. We also went back and double checked by hand in ds9 as shown in 6.

We then outputted the information to new data frames, while including a criterion to reject any stars that lied within 25 pixels from the edge of frame. This was to prevent using data skewed by stars only partially in a frame, since our stars moved slightly when each image was taken at the telescope. Below is a few column entries from the light curve data frame for our first reference star, the data we mainly worked with in figure ?? is Aperture Flux, its error, and the times.

We generated 11 total data frames, including one for HAT-P-6. Each one is variable in rows, containing different amount of data points, they are also not solved in order by sextractor, so it is in randomized order as seen above. However, reference stars 5 and 7, were unsolvable by sextractor. Leaving us with a total of 8 reference stars.

3.4. Reference star Light Curves

3.4.1. Raw Data Plotting

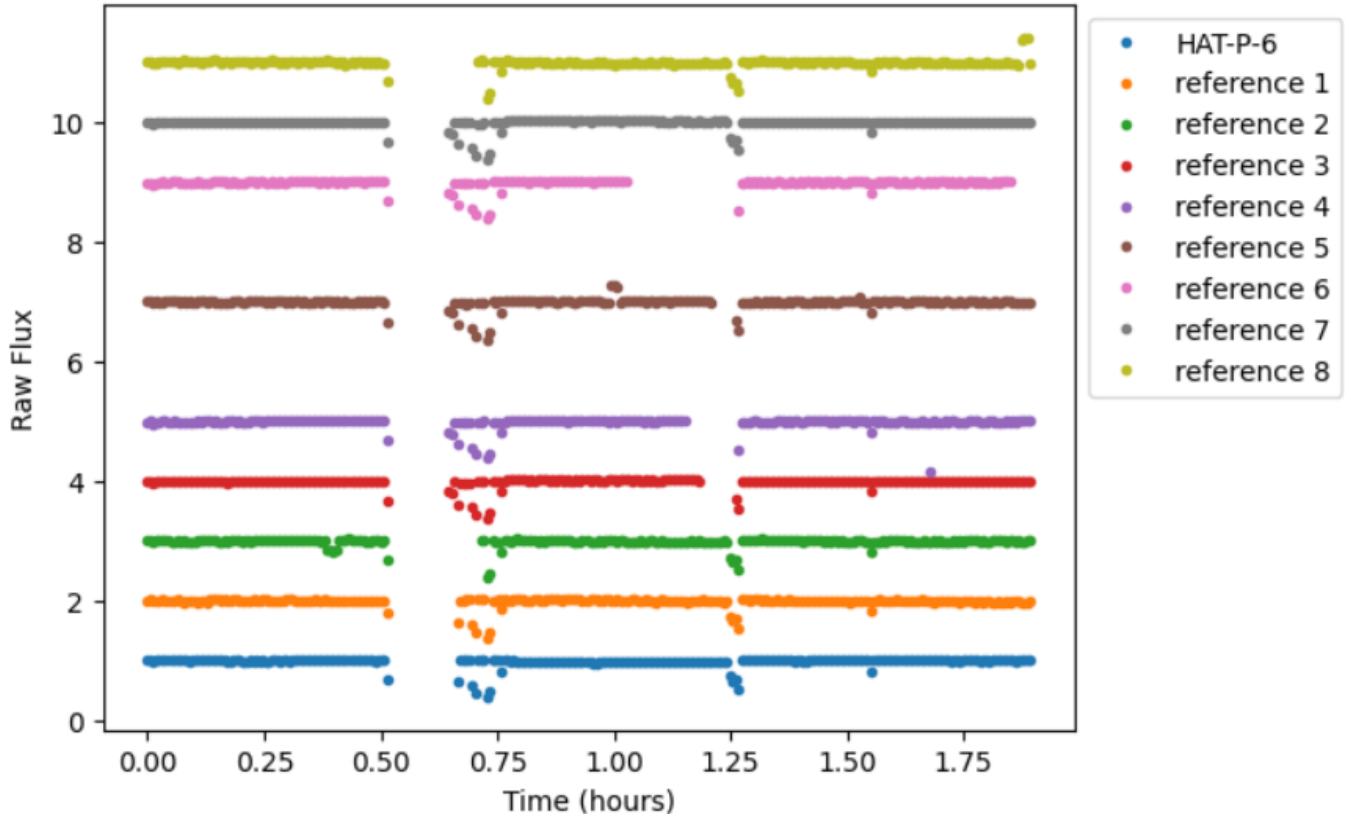
Here is the plotting of our raw and uncalibrated light curves for the 8 reference stars, and HAT-P-6 on the next page. It was calculated by plotting every aperture flux value at every time in each data frame, divided by the median of the aperture flux of the respective star. Although still uncalibrated, this normalizes the data and enhances the visual interpretations by making relative flux variations more evident. And of course normalization helps reduce any systematic noise we may encounter in the data.

The meridian flip is now evident, at around the 30 minute mark, corresponding with our recorded notes on the experimentation [can be found in the Jupyter notebook code]. And there is another discrepancy around the 1 hour 15 minute mark, which is when we made our large telescope movement to recenter HAT-P-6 in the

Figure 9. reference star 1 light curve data frame

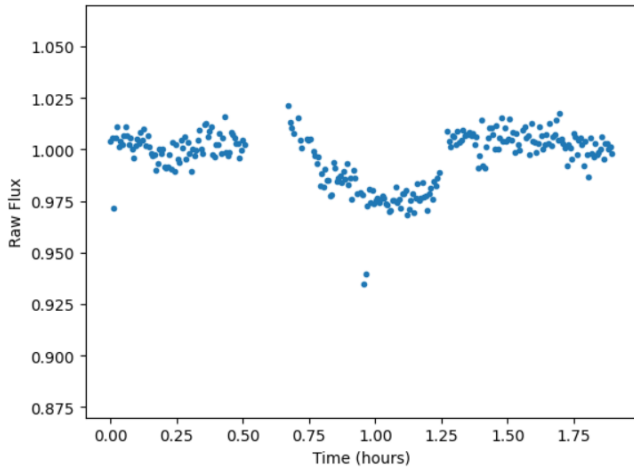
	object_index	x	y	barycenter_ra	barycenter_dec	aperture_flux	aperture_flux_error	time	flux_radius	gaussian_f	background	threshold	flux_max	isoarea_image	prof_rms_r	prof_rms_r	pos_angle	flags
146	147	800.6921	171.031	354.601019	42.5029876	10750.49	105.4099	0	1.363	2.59	63.30581	24.78594	1368.003	41	1.29	1.029	-50.96	0
147	148	798.7162	173.6994	354.601021	42.5030133	10954.11	105.4855	0.0063	1.321	2.63	62.86795	24.76867	1422.204	43	1.267	1.115	-81.13	0
147	148	780.8467	198.5398	354.600098	42.5029703	10932.16	104.6573	0.0633	1.333	2.67	60.55962	24.60026	1438.25	37	1.234	0.998	-45.2	0
123	124	29.7165	544.7089	354.601093	42.5029889	6781.501	103.7023	0.665	1.26	2.4	56.64621	24.34997	907.1151	31	1.137	0.941	-18.12	0
96	97	32.7771	541.9953	354.601048	42.5030333	10507.33	103.2362	0.6713	1.321	2.52	56.55949	24.27481	1388.522	36	1.158	1.021	-73.83	0
93	94	35.5535	539.627	354.601115	42.5032476	10628.95	103.2625	0.6777	1.158	2.09	56.79553	24.26812	1521.958	33	1.028	0.981	-88.65	0

Figure 10. 6 pixel Raw light curves of all stars



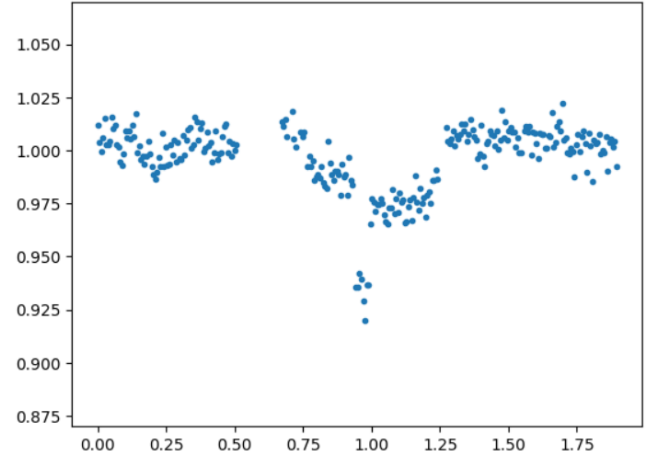
center along with the 10 reference stars. The variations due to atmospheric variability and intrinsic brightness variability in the stars are evident by the random outliers despite having corrected for readout noise and other variables by the dark and flat field frames.

Figure 11. uncalibrated 6 pixel HAT-p-6 light curve



We will now discuss the aforementioned 6 pixel and 11 pixel variations in the data. For the sake of redundancy,

Figure 12. uncalibrated 11 pixel HAT-p-6 light curve



the uncalibrated raw light curve will only be represented by the 6 pixel graph, they are quite similar given smaller outliers. The calibrated has more implications and will be provided otherwise. Here are both pixel graphs of a large scale focus of HAT-P-6's light in order to understand the unfiltered data, variations, and how flux calibrations are going to eventually effect the data skew. The graphs were produced in the same manner as the above light curve graphs, but just limiting the y-scale

to precisely observe the pixel variations in the HAT-P-6 curves for comparison between the aperture radii.

As we can see they share similar density profiles, the 11 pixel aperture contains more outliers, this is to be expected as we are enlarging our capturing radius therefore yielding more potential outliers. Below are the associated error bars for both graphs, they are almost identical which is to be expected as uncalibrated data implies that the errors most likely reflect noise rather than signal variations. Due to the nature of the raw data obviously not accounting for calibrations that are noise dependent and aperture dependent [Howell \(1989\)](#). As we can see the error bars are nearly invisible, this was to be expected as our values had very small associated error values, for example, HAT-P-6 had around 50,000 counts ± 100 counts. The error bars were easily accessible using the intrinsic functions of matplotlib (`ax.errorbar`).

3.4.2. Calibrating and Rescaling Reference Stars

Now we will discuss the calibration of our Reference stars. The lab manual provides this equation in order carry out our rescaling of fluxes.

$$f_j(t) \rightarrow \frac{f_j(t)}{\langle f_j \rangle}; \sigma_{f_j(t)} \rightarrow \frac{\sigma_{f_j(t)}}{\langle f_j \rangle} \quad (3)$$

Both of these represent the flux and error rescaled by dividing out the length of the observation from each star's average flux [Birrner \(n.d.\)](#). We removed all potential stars that portray large variability, and because we had a large telescope movement as well as meridian flip, we individually identified all frames that contained streaked or smeared images and removed in this step. We set our threshold of "outliers" as anything outside one standard deviation away from the data.

we started off by calculating the rescaled flux represented by equation 3's $f_j(t)$, and then removed it if its difference between its median is greater than its "one standard deviation $\sigma_{f_j(t)}$ ". Also removing any rows whose time values are within .0006 of the smeared frames values. This process was also done for HAT-P-6. And we plotted all the "cleaned and rescaled" light curves to better visualize the new density profile.

The graphs for both 6 pixel and 11 pixel aperture radius are provided below. Again we can see much higher variation or uncertainty in the 11 pix light curves, as expected. However a unique development is that the density profiles of certain curves behave opposing to others right after the meridian flip.

Figure 13. 6 pix error bars

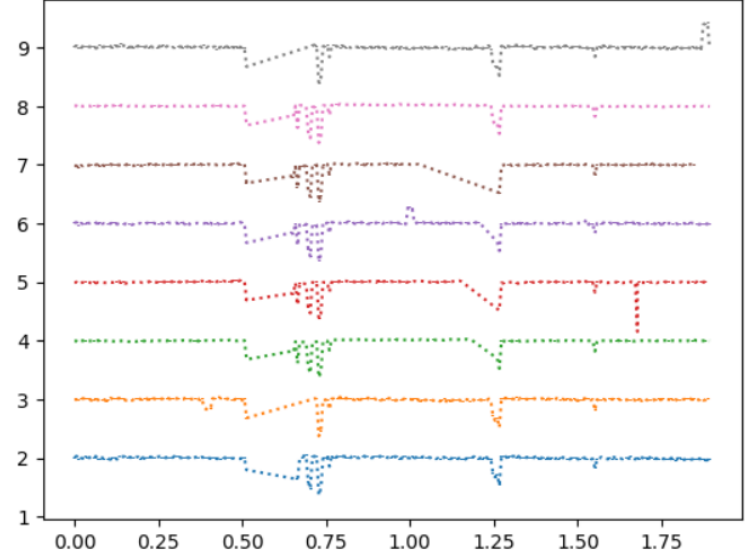


Figure 14. 11 pix error bars

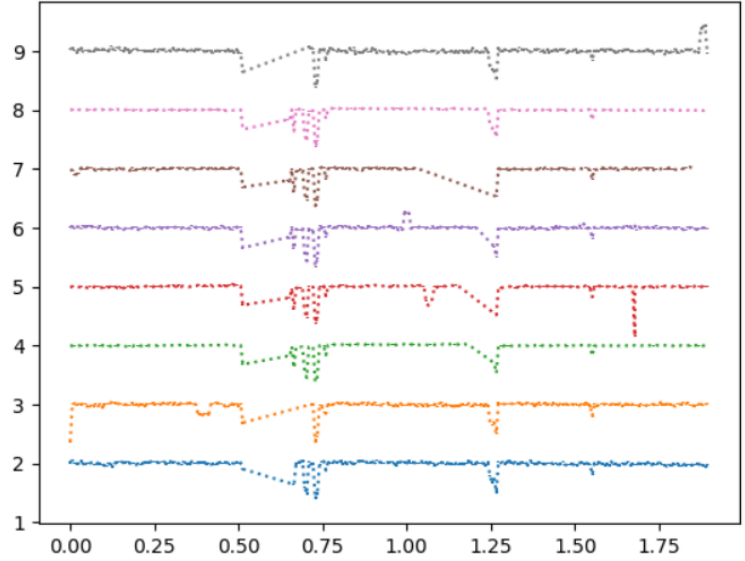


Figure 15. 6-pix rescaled/cleaned Light Curves

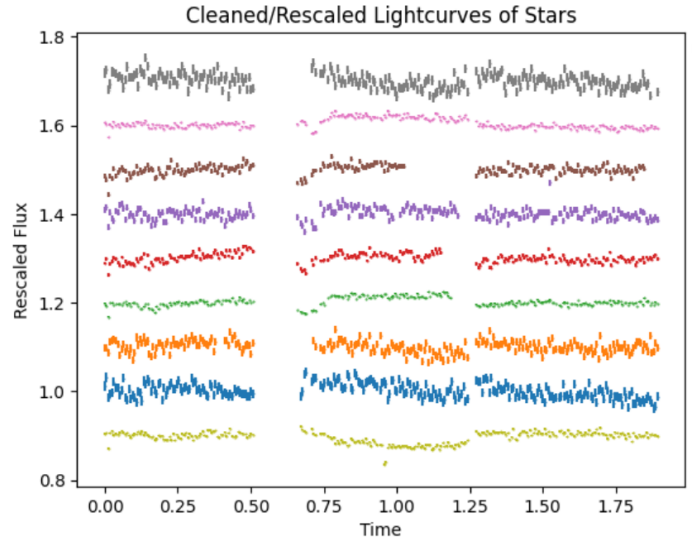
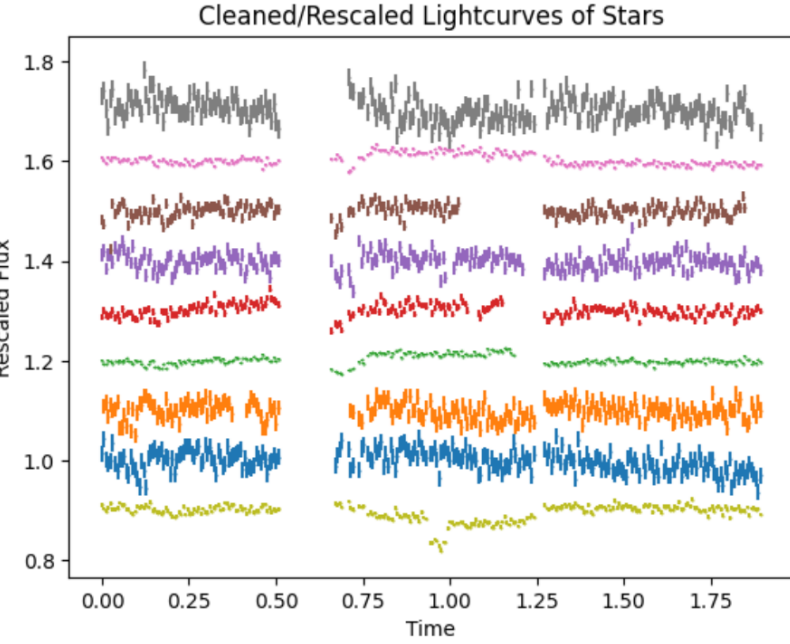


Figure 16. 11 pix rescaled/cleaned Light Curves

The more variable stars curve up and then back down, while the more consistent stars, including HAT-P-6, which still the bottom curve, curves down and then upwards. This will be discussed in more detail in the results.

3.5. Finally, a light curve?

In this section we finally calculate our target star, calibrated, light curve. The calibrated reference star light curves now provide us the information on atmospheric change, finally representing the calibration data we need in order to correct HAT-P-6's light curve. The Lab manual provides two equations, for calculating average flux using a weighted mean. The purpose of this is that by averaging over all the star flux's, we can obtain the relative Flux for our target star. A weighted mean prioritizes preserving our data by giving lower uncertainty data more value, essentially rendered the skewed data ineffective.

$$\mu_i^{\text{ref}} = \frac{\sum_j f_j^{\text{ref}} / (\sigma_j^{\text{ref}})^2}{\sum_j 1 / (\sigma_j^{\text{ref}})^2} \quad (4)$$

And the below equation, also from the lab manual, is the error of the weighted average flux Birrer (n.d.).

$$\sigma_i^{\text{ref}} = \sqrt{\frac{1}{\sum_j 1 / (\sigma_j^{\text{ref}})^2}} \quad (5)$$

We now calculate our baseline flux. We started by creating a fresh data frame to hold all the cleaned reference star's data. We then run through all the reference times

and compare to the target star's data times, using a tiny threshold, if the criteria is met then the reference star's flux and uncertainty is added to the data frame. We then calculate the weighted uncertainty and reject any flux values outside of double the weighted uncertainty. After calculating the weighted means of the remaining flux values, as well their uncertainties, we create a final data frame with time, weighted mean of the reference stars' flux, and uncertainty columns and their respective data values.

We then rescaled the target star's flux and error by its median flux to ensure consistency across all frames. We then found the ratio between HAT-P-6's flux and the weighted mean's of the reference star flux by dividing them, and propagating the error for the ratio using quadrature. The flux ratio and error is then normalized by the mean of HAT-P-6' flux, but only for time after 1.6 hours, in order to obtain the proper baseline flux of our star. We don't look at any other data for the baseline due to the fact that we missed the start of the transit, so therefore have no data prior to it. We encountered some rows in the weighted flux error of the rescaled data frames that had "infinite error", so we rejected all the rows that had error quality.

We obtained the calibrated light of Hat-P-6 by plotting ratio between baseline over average flux for each time, and this was run for both 6 pixel and 11 pixel aperture radii of course. Here are the plots of both final light curves of HAT-P-6, included unbinned data to show the associated error

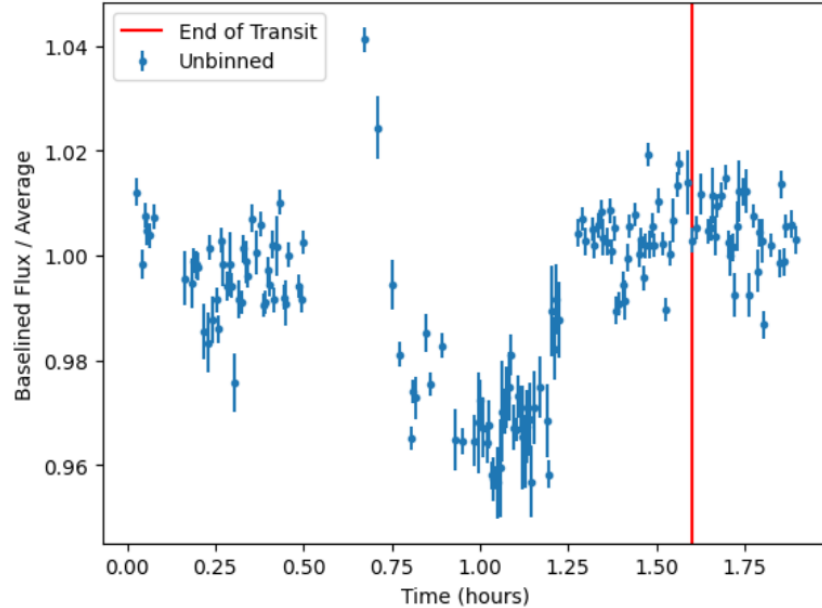
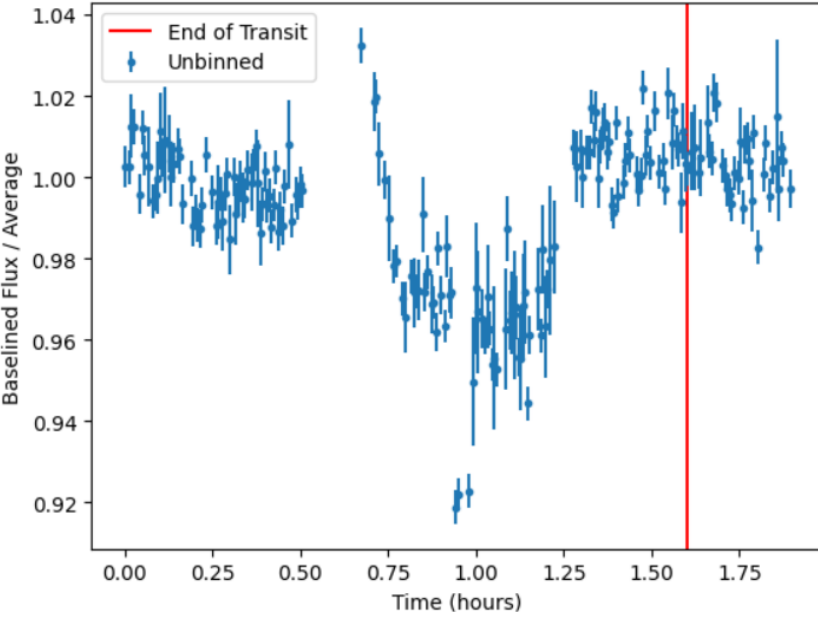
Figure 17. Calibrated HAT-P-6 light curve for 6 pixel aperture radius

Figure 18. Calibrated HAT-P-6 light curve for 11 pixel aperture radius



4. RESULTS AND DISCUSSION

The final light curves for both aperture radius raise fundamental questions in the nature of our data. The purpose of our aperture radius difference was to check the relationship between our Noise values and validity of our data. However Despite calibration and correcting for various factor, we obtained a density profile very similar to the one prior to correcting our reference stars. The gap in the meridian flip was expected, however the jump in data it causes for both aperture radii is concerning in regards to the validity of our light curve. The profile in appearance has both an ingress and a digress, which normally would be very positive indications of exoplanet transit detection, but unfortunately our first image was not until we after the ingress. According to swarthmore, the transit midpoint was at 10:54, and our primary photometric image wasn't even until 10:59. The transit ended at 1.6 hours marked by the red line. This means that our profile should be the egress, or half a transit. However after the maridian flip, we are observing "full transit" behavior, as well as a major data gap around 1.3 hours.

It is worth mentioning again that was during the time we made our biggest telescope movement to readjust the position of our stars to keep them in frame. The profiles of our reference stars also are peculiar in that half the stars observe a certain profile and the other half follow a different motion. HAT-P-6 seems to follow the profile of the stars with less uncertainty, this makes sense as the lower uncertainty stars are worth more weight

in weighted mean calculations. But the final calibrated light curve is inconclusive in results. We are unable to make a reasonable assumption that we have detected a exoplanet. We are at this time unable to calculate the transit time given our lack of data. Although we calculated planetary to solar radius ratio, given that our transit depth information is in adept, it is highly unreliable, and cannot be assumed to be valid data nor can we draw any conclusions. We have calculated improbable values for percent change in Flux as well as transit depth as mentioned.

4.1. Percent change in Flux

We went ahead and calculated our transit depth as well percent change in flux dips. We started initially by finding the baseline normalized flux ratio during and after our transit to calculate the percent change. We found the weighted mean by summing the flux values divided by the variance, all over the sum of the inverted variances in order to get that weighted value. This was done twice, before 1.6 hours and after, which is the time that marks our transit ending.

$$\text{during_transit_mean} = \frac{\sum_i \frac{F_i}{\sigma_i^2}}{\sum_i \frac{1}{\sigma_i^2}}, T < 1.6 \quad (6)$$

$$\text{after_transit_mean} = \frac{\sum_i \frac{F_i}{\sigma_i^2}}{\sum_i \frac{1}{\sigma_i^2}}, T > 1.6 \quad (7)$$

We then found the error of these values as the square root of the inverse sum of inverted variance

$$\text{during_transit_error} = \sqrt{\frac{1}{\sum_i \frac{1}{\sigma_i^2}}}, T < 1.6 \quad (8)$$

$$\text{after_transit_error} = \sqrt{\frac{1}{\sum_i \frac{1}{\sigma_i^2}}}, T > 1.6 \quad (9)$$

For the 6 pixel aperture radii, The values came out be:

- during: 0.99516 ± 0.00497
- after: 1.0048 ± 0.00966

For the 11 pixel aperture radii, The values came out be:

- during: 0.99190 ± 0.00564
- after: 1.0023 ± 0.0120

Both aperture radii results have a percent difference of 1%. However based on the skew of the data for both graphs, we can assume it is inconclusive that these values as correct

4.2. transit depth

We calculated our transit depth by taking the difference of the weighted averages of the transit flux values. here was our result and associated error which was calculated by taking the square root of the sum of the squared errors.

$$\text{depth error} = \sqrt{(\text{during}(\text{error}))^2 + (\text{after}(\text{error}))^2} \quad (10)$$

our transit values for both aperture radii came out to:

- 6 pixel: 9.565 ± 10.862 ppt
- 11 pixel: 10.44 ± 13.26 ppt

Our Swarthmore value is 9.1 ppt. This paper: [Investigating giant planet migration history](#), implies an area ratio of 0.0088 ± 0.00054 , which agrees with Swarthmore's value. Although we obtained values relatively close, the uncertainties are quite large, this could be due to the fact the values we worked with are in the 4-5 orders of magnitude range, so there is small associated error per value. But when you obtain a very small difference, there is now a relatively large error associated with small difference value.

4.3. planetary radius

This [website](#) provides a reference for calculating the planetary to solar radius ratio, and says it is given by: $D = (\frac{R_p}{R_s})^2$ Using our transit depth, that would yield an upper limit ratio of 0.094. This is very close to the literature value 0.095 for HAT-P-6 to HAT-P-6b (Noyes, R. W.). However we can only take it as an assumption given that our transit depth uncertainty was quite high,

as well the validity of the depth itself being very low given the skewed light curve for Hat-P-6.

5. CONCLUSION

Despite discovered a light curve that faked the appearance of a transient dip, we cannot assume that we have discovered nor verified the existence of HAT-P-6b at this time. We were unable to confirm our final planetary radii value and transit time due to lack of data and the lack of ability to verify its validity, despite obtaining a ratio of 0.0094, which is about a 1% percent error. We were also able to calculate a percent change in flux as well as a transit depth, that both fall within the accepted literature value, but once again the probability of their validity is quite low. Our transient depth came out to be 9.565 ± 10.862 ppt for the 6 pixel aperture radius, and 10.44 ± 13.26 ppt for 11 pixel. Our biggest sources of error seem to result from the motion of the telescope, mainly the meridian flip seemed to cause unruly behavior in the density profiles of the references stars, creating unique profile motion for different stars. As well as moving the telescope around, seemed to create large jumps in flux values rather than just remaining as a "hole" in the slew of data. Due to these struggles, and the fact that we were not able to start recording images until after the midpoint of the transit, we are unable to verify whether our transit was discovered or not due to the nature of our final light curve, despite that exceptionally close transient depth, planetary to solar radius ratio, and percent change in flux values that we came to find. We must conclude an nonconclusive result, assuming that our resulting values are products of artifact processing or even coincidental.

REFERENCES

- Birrer, S. ????, Observing Equipment, AST443/PHY517 Wiki, https://github.com/sibirrer/PHY517_AST443/wiki/Observing-Equipment
- . n.d., Transit Planet Lab Manual
- Charbonneau, D., et al. 2000, The Astrophysical Journal, 529, L45, doi: [10.1086/312457](https://doi.org/10.1086/312457)
- Greisen, E. W., & Calabretta, M. R. 2002, Astronomy and Astrophysics, 395, 1061
- Howell, S. B. 1989, Handbook of CCD Astronomy (Cambridge University Press)
- Noyes, R. W., Bakos, G. Á., et al. 2008, The Astrophysical Journal, 673, L79, doi: [10.1086/528792](https://doi.org/10.1086/528792)